Surface Step Effects on Nanoindentation

J. A. Zimmerman, C. L. Kelchner, P. A. Klein, J. C. Hamilton, and S. M. Foiles

Sandia National Laboratories, MS 9161, P.O. Box 969, Livermore, California, 94551-0969

Atomistic simulation is used to examine nanoindentation of a Au(111) crystal both near and far from a surface step. While the load needed to nucleate dislocations decreases significantly when indenting close to the step, the extent of the step's influence is not as great as seen experimentally. This behavior is explained by measuring the contact area from the simulation data. A new metric, the slip vector, shows material slip coinciding with the $\langle 112 \rangle$ directions of a lowest unstable stacking fault barrier. The slip vector is used to calculate an atomic critical resolved shear stress, which is shown to be a good dislocation nucleation criterion.

The indentation of a crystal by a hard, nanometer-sized object is a benchmark problem for determining critical energies and stresses needed for defect creation and propagation within materials. Indentation has been rigorously treated in isotropic elasticity [1] and extensively studied in experiments at the nanoscale [2–4]. Few of these experiments have produced information about the initial formation of dislocation loops, which signifies the onset of plasticity. Kiely *et al.* [5] observed in experiment that surface steps play a role in the development of dislocations, as the amount of load necessary to create dislocations lessens when the indenter is close to these steps. Our objective is to use atomistic simulation to gain knowledge about how surface geometry affects dislocation formation. We perform a series of simulations of a Au(111) crystal with indentation at various distances from a surface step. A new deformation parameter, the slip vector, is used to quantify the dislocation content of nanoindentation defects. It is used with the atomic stress fields to determine the critical amount and direction of resolved shear stress (CRSS) necessary for dislocation nucleation. Our simulations reveal that physical contact between an indenter and a surface step is sufficient to explain a drop in indentation force when the indenter is close to the step, altering the details of dislocation nucleation without necessarily changing the magnitude of the CRSS. This magnitude is observed to vary only in cases of high deformation or where the crystallography conflicts with the surface step geometry. A contact-based geometrical expression is used to explain both simulation results and experimental data.

A number of simulations of nanoindentation have been performed in recent years. Robertson and Fivel [6] compared dislocations produced from experimental nanoindentation of Cu(100) with those seen in a dislocation dynamics simulation with boundary conditions dictated by isotropic elasticity and the finite element method. At the atomic scale, Tadmor *et al.* [7,8] used the quasicontinuum method to study two-dimensional nanoindentation from a rigid punch. These simulations led to several insights about the contribution of image forces and surface energies to dislocation nucleation; however, the types of dislocations formed were restricted by the geometry of the simulation region. These restrictions no doubt alter any estimation of the CRSS. Kelchner *et al.* [9] used a repulsive potential to model a spherical indenter penetrating the passivated surface of a Au(111) crystal modeled with the embedded atom method (EAM) [10]. This work showed that complex dislocation loops formed within the crystal and grew to intercept the crystal surface. Visualization of dislocations and stacking faults, a difficult task accomplished by only a few researchers [11], was achieved by the development of the centrosymmetry parameter.

In this Letter, atomistic simulations of nanoindentation were performed on a 199 Å wide by 400 Å long by 125 Å thick single crystal containing approximately 560 000 atoms. The top surface was traction free and contained a step-one atomic layer in height through the width. The bottom surface was held fixed while periodic boundary conditions were applied to the side surfaces. The crystal was composed of gold modeled with EAM potentials [10]. The attributes of these potentials will be discussed towards the end of this Letter. The fcc crystal was oriented such that the top surface was the (111) plane, and the step was oriented along the $[1\bar{1}0]$ direction, perpendicular to the $[11\bar{2}]$ direction. Two different step orientations were used, (i) $\langle 110 \rangle / \{100\}$ and (ii) $\langle 110 \rangle / \{111\}$ [12], because of the threefold symmetry of the (111) surface. The same repulsive potential used in [9] emulated a spherical indenter of tip radius $R = 40$ Å. The indentations were performed quasistatically at zero temperature using the conjugate gradient method [13]. The indenter was lowered in increments ranging from 0.1 to 0.5 Å. The indenter center was positioned at various distances d from the surface step, on both the low and high sides, respectively defined as $d < 0$ and $d > 0$.

A tensor variable used in the analysis of atomistic simulations is the atomic stress. The theorems developed by Clausius [14] and Maxwell [15] relate the Cauchy stress tensor $\boldsymbol{\sigma}$ applied to the boundary of a volume containing atoms to the kinetic motion and interatomic forces between those atoms. This relation is used to define local atomic stress, for which $\boldsymbol{\sigma}$ is the ensemble average.

To provide information on the Burgers vectors of dislocations, we developed the slip vector, defined as

$$s^\alpha = -\frac{1}{n_s} \sum_{\beta \neq \alpha}^{n} (x^{\alpha\beta} - X^{\alpha\beta}).$$ (1)

In this expression, n is the number of nearest neighbors to atom α, n_s is the number of slipped neighbors, and $x^{\alpha\beta}$ and $X^{\alpha\beta}$ are the vector differences of atoms α and β current and reference positions, respectively. The reference configuration is the arrangement of atomic positions associated with zero mechanical stress. Although the term "slip vector" has been used as a synonym for the Burgers vector [16], in the present context its meaning is given by (1). This expression will result in the Burgers vector for the slip of adjacent atomic planes, where the atom lies on one of those planes. The slip vector will have a large magnitude for any inhomogeneous deformation near an atom and will provide quantitative information about the deformation. The slip vector can be used for any material microstructure, making it more generally applicable than the centrosymmetry parameter [9].

In the simulations, data were accumulated for several force-depth curves, such as those seen in Fig. 1. For distances far from the step where $|d| \geq 20$ Å, elastic Hertzian behavior persists until a yield load F_y is reached at a penetration depth δ_y and dislocations are nucleated upon further loading. This nucleation is characterized by a drop of 30% to 40% in indentation load. Although their elastic responses are identical, once dislocations are generated the load behavior differs for A and B steps due to the difference in the orientation of their slip systems. Similar behavior is seen for indentation near a surface step, although a reduced stiffness is observed and either a small drop of less than 15% in load or an appreciable change in slope of the force-depth curve characterizes the yield load. Figures shown in this paper will display data both at loads corresponding to the "initial event," which indicates the first formation of dislocations, and at load drops. The features shown in Fig. 1 are qualitatively similar to those seen in experiment [5], although load drops for indentation
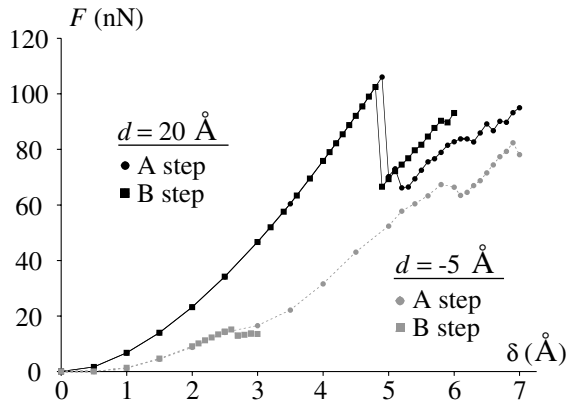
far from a step are more extreme in experiment, producing nearly complete unloading.

When indenting far from a step, F_y approximately equals 105 nN. F_y decreases when the indenter is centered less than 20 Å from the step, down to values between 10 and 20 nN. The lowest yield loads are observed when -10 Å $\leq d \leq 0$. To interpret this behavior, the surfaces of these systems were viewed with atoms colored according to whether or not they were in contact with the indenter tip. A few of these images are shown in Fig. 2, and reveal that a portion of the contact area lies on the step when the indenter is positioned on the low side of the step. For $|d| \leq 20$ Å, contact with the step alters the load necessary to nucleate dislocations. The most extreme situations occur in frames 2(c) and 2(g), in which all of the initial contact occurs on the step edge, although the indenter is centered off-step. These images were used to estimate the contact area and a contact radius a_y at the onset of dislocation formation. Figure 3 shows F_y as a function of distance from the step normalized by a_y. F_y decreases abruptly at normalized distances closer than 1.5, with the most prominent effects felt at distances closer than or equal to 1.

Figures 2 and 3 suggest that caution should be used when estimating the contact area in order to calculate mean pressure beneath the indenter, $\sigma_y = F_y/(\pi a_y^2)$. Experimental measurements [5] showed σ_y decreasing significantly for values of $|d/a_y| < 3$, indicating a long-range effect of the step. However, those values were obtained by calculating contact area with the Hertzian relation $a_y = \sqrt{R\delta_y}$. Use of this relation at the nanoscale is questionable, as a_y is not as well defined near a step. In our simulations, the surface step causes a significant variation in the values of σ_y for normalized distances less than 1.5, although this variation does not necessarily show a downward trend as $|d/a_y|$ approaches zero.

Also, those experiments used steps that varied in height from 5 to 30 Å. The distance from the step at which a spherical indenter first contacts both the planar surface and the step edge (d_c) can be geometrically estimated to equal
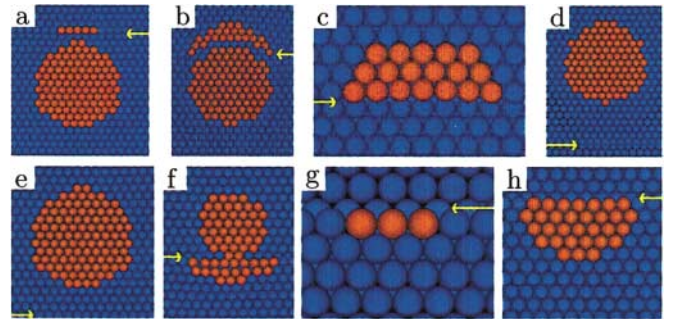

FIG. 1. Indentation force as a function of depth for both types of steps at different distances from the step.

FIG. 2 (color). Contact area at the yield load for the A step at distances $d =$ (a) -20 Å, (b) -10 Å, (c) -5 Å, (d) 30 Å and for the B step at distances $d =$ (e) -30 Å, (f) -10 Å, (g) -5 Å, (h) 0. Yellow arrows highlight the position of the step line.
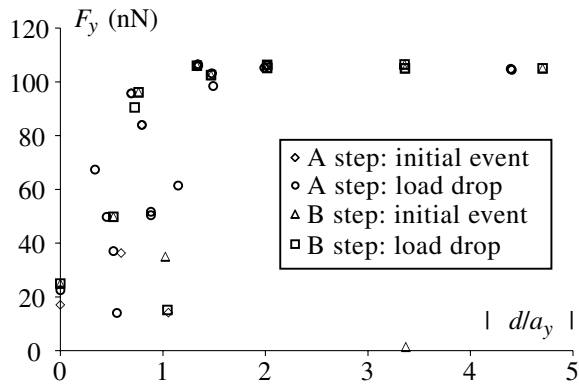
FIG. 3. Indenter load at initial plasticity events and load drops as a function of distance from the step normalized by contact radius.

$d_c = \sqrt{2Rh - h^2}$, where h denotes the step height. The purpose of determining d_c is to show that if a step effect, such as a load drop, is noticed at $d < d_c$, the effect is due to direct contact between the indenter and the step. If such an effect is noticed at $d > d_c$, then contact alone cannot account for it. For our simulations, if the undeformed value of $h = 2.36$ Å is used, $d_c = 13.5$ Å. However, if an "effective" height $h_e \equiv h + \delta_y$ is used and $\delta_y = 4.4$ Å, then $d_c = 22.2$ Å. This agrees with the observations of both step types in Fig. 2 which show no contact at $d = -30$ Å but some contact at $d = -20$ Å. When $d \approx d_c$, $a_y \approx 15$ Å and $|d_c/a_y| = 1.48$. Experimental values of R (2300 Å), h (28 Å), and δ_y (34 Å) for the near-step indentation shown in Fig. 2(b) of [5] yield $d_c = 358$ Å using h and 530 Å using h_e, both of which are larger than the measured distance $d = 300$ Å. Thus, the estimate of d_c shows that the indenter actually hits the step, acting as a stress concentrator, rather than the step having a long-range effect. Using the Hertzian relation produces $a_y = 280$ Å and $|d_c/a_y| = 1.28$ (h) or 1.9 (h_e).

Analysis of the dislocation structures produced during indentation leads to a greater understanding of their nucleation. Figure 4 displays typical dislocation loops pro-
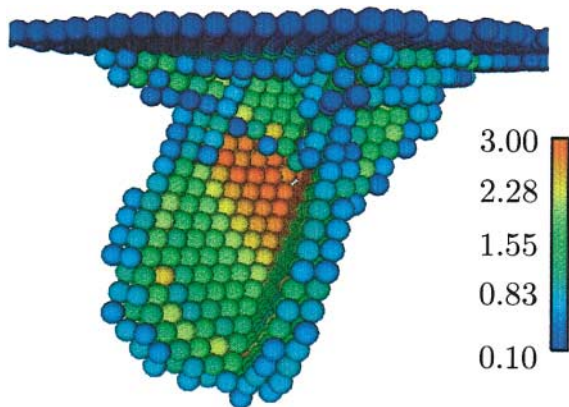
duced after the load drop for indentation far from the steps. The slip vector magnitude in stacking fault regions, colored green, is 1.662 Å, which is very close to the value for a $\langle 112 \rangle$ partial dislocation in gold (1.666 Å), and the value in regions traversed by a full dislocation, colored red, lies between 2.7 and 3.0 Å, consistent with the magnitude of a $\langle 110 \rangle$ vector (2.885 Å). Slip vector components allow identification as to which specific partial dislocation is nucleated on a {111} plane.

The planes on which dislocation loops develop change as the indenter approaches the step. Figure 5 shows dislocation structures nucleated when the indenter is at $d = -5$ Å and at $d = 0$. Images for the A step show a loop formed on the $(\bar{1}\bar{1}1)$ plane, the inclined plane intersecting the surface along the step edge direction, $[1\bar{1}0]$. Although loops grow on this plane for both distances, the slip direction is $[\bar{2}1\bar{1}]$ for $d = -5$ Å and $[1\bar{2}1]$ for $d = 0$. For the B step, the $(\bar{1}\bar{1}1)$ plane is oriented opposite to the way it is for the A step. Thus, the resulting structures possess radically different shapes which are several atomic layers thick and oriented in the inclined $[\bar{1}10]$ direction, coinciding with most of the atoms' slip vectors. Clearly, the structures that have developed near the surface step are highly influenced by the crystal orientation.

The slip vector is used with the atomic stress tensor to estimate the CRSS required for dislocation nucleation. Most nanoindentation research has used either the maximum RSS or the largest RSS for a $\langle 110 \rangle$ or $\langle 112 \rangle$ direction. However, the slip vectors measured in our simulations show that, while slip does occur in $\langle 112 \rangle$ directions, the direction of slip rarely corresponds to the direction of the largest RSS. For indentation far from a step, the atomic RSS for slip directions reaches a maximum of 3.26 GPa prior to dislocation nucleation, even though a higher value of 6.32 GPa occurs for a different $\langle 112 \rangle$ direction. Slip occurs in the lower RSS direction due to a lower energy barrier for sliding of atomic layers past each other. The height of this barrier, known as the unstable stacking fault energy γ_{us} [17], has been shown to be asymmetric with regard to the direction of slip [18]. The orientation of our crystal is such that slip occurs when the RSS is 3.26 GPa in the direction of this lower energy barrier. Thus, any

FIG. 4 (color). Dislocation loops nucleated for indentation far from the surface steps, with atoms colored by $|s^\alpha|$.
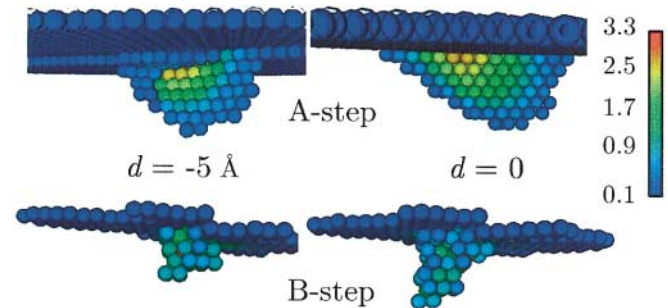

FIG. 5 (color). Dislocation loops nucleated for indentation close to the surface steps, with atoms colored by $|s^\alpha|$.

nucleation criteria within a material model should not only contain a critical amount of stress but also contain the direction and sense of the slip.

Some of our simulations were repeated using EAM potentials [19] that produce a value for intrinsic stacking fault energy, γ_{sf}, closer to the experimental value of $32-33$ mJ/m^2 [20–22]. These simulations show little difference ($\lesssim 13\%$) in the experimentally relevant quantities of F_y and δ_y as compared with the original runs, and display the same step effect. This is because the value for γ_{us} is almost identical for the two potentials, 103 and 102 mJ/m^2, both of which compare well with the density functional theory prediction of 140 mJ/m^2. Only characteristics related to γ_{sf}, such as partial dislocation loop size, differ between simulations.

The CRSS observed far from a step is nearly constant for distances as close as 5 to 10 Å from the step. Data for the A step show a decrease in this value, down to 2.21 GPa, for the simulations where $|d| \leq 5$ Å, which may be caused by the very large deformations which affect γ_{us} [23], or by image force effects that are more prominent when dislocation nucleation occurs at a step edge [18]. Near the step, the B step data show a higher CRSS for cases in which the slip direction is not a $\langle 112 \rangle$ direction, as depicted in Fig. 5. Nevertheless, our observations show that the value of CRSS remains roughly constant for similar types of slip directions even though the specific combination of slip plane and Burgers vectors changes.

The value of CRSS far from the step is very close to the theoretical shear strength of this EAM potential, $\frac{\mu}{2\pi} = 3.66$ GPa. Experimentally determined estimates of the CRSS range from 1.5 to 2 GPa [2,3], roughly half the value observed in simulation. This level of agreement is significant considering that experimental dimensions and loads are 2 to 3 orders of magnitude higher than those used in simulation. Any discrepancy may be due to a size scale effect, which would lead to a more inhomogeneous deformation state beneath the indenter, and influence the degree that image forces affect nucleation. Our simulations were performed at zero temperature, whereas the experiments referenced were done at room temperature. The effect of temperature on the dislocation nucleation process is not well understood. In both experimental [24] and theoretical [25,26] studies, stacking fault energies show little dependence on temperature below 400 K. However, theoretical models of dislocation emission from a crack tip show a definitive relationship between activation energy and temperature [25,27]. Although further study of finite temperature dislocation formation is warranted, our results can be considered a successful first attempt at understanding the mechanics of dislocation emission during nanoindentation, and how surface geometry affects this process. These de-

tails are important for other materials' problems such as thin-film heteroepitaxy and ductile crack propagation. The slip vector will no doubt be useful for studying these phenomena as well.

---

[1] K. L. Johnson, *Contact Mechanics* (Cambridge University Press, Cambridge, UK, 1985).

[2] S. G. Corcoran *et al.,* Phys. Rev. B **55**, R16057 (1997).

[3] J. D. Kiely and J. E. Houston, Phys. Rev. B **57**, 12 588 (1998).

[4] J. D. Kiely *et al.,* J. Mater. Res. **14**, 2219 (1999).

[5] J. D. Kiely, R. Q. Hwang, and J. E. Houston, Phys. Rev. Lett. **81**, 4424 (1998).

[6] C. F. Robertson and M. C. Fivel, J. Mater. Res. **14**, 2251 (1999).

[7] E. B. Tadmor, R. Miller, and R. Phillips, J. Mater. Res. **14**, 2233 (1999).

[8] V. B. Shenoy, R. Phillips, and E. B. Tadmor, J. Mech. Phys. Solids **48**, 649 (2000).

[9] C. L. Kelchner, S. J. Plimpton, and J. C. Hamilton, Phys. Rev. B **58**, 11 085 (1998).

[10] S. M. Foiles, M. I. Baskes, and M. S. Daw, Phys. Rev. B **33**, 7983 (1986).

[11] S. J. Zhou *et al.,* Phys. Rev. Lett. **78**, 479 (1997).

[12] S. Liu *et al.,* Phys. Rev. Lett. **71**, 2967 (1993).

[13] W. H. Press, *Numerical Recipes: The Art of Scientific Computing* (Cambridge University Press, Cambridge, UK, 1989).

[14] R. J. E. Clausius, Philos. Mag. **40**, 122 (1870).

[15] J. C. Maxwell, Trans. R. Soc. Edinborough **XXVI**, 14 (1870).

[16] L. H. Van Vlack, *Elements of Materials Science and Engineering* (Addison-Wesley, Reading, MA, 1980).

[17] J. R. Rice, J. Mech. Phys. Solids **40**, 239 (1992).

[18] J. A. Zimmerman, Ph. D. thesis, Stanford University, 2000.

[19] D. L. Medlin, S. M. Foiles, and D. Cohen (to be published).

[20] M. L. Jenkins, Philos. Mag. **26**, 747 (1972).

[21] T. J. Balk and K. J. Hemker, Phil. Mag. A **81**, 1507 (2001).

[22] The original potential used yields $\gamma_{sf} = 5$ mJ/m^2, while the one from [19] produces a value ≈ 31 mJ/m^2.

[23] J. A. Zimmerman, H. Gao, and F. F. Abraham, Model. Simul. Mater. Sci. Eng. **8**, 103 (2000).

[24] T. Imura and H. Saka, *The Structure and Properties of Crystal Defects* (Elsevier, New York, 1983), p. 91.

[25] Y. W. Zhang, T. C. Wang, and Q. H. Tang, J. Phys. D **28**, 748 (1995).

[26] M. de Koning *et al.,* Phys. Rev. B **58**, 12 555 (1998).

[27] K. S. Cheung, A. S. Argon, and S. Yip, J. Appl. Phys. **69**, 2088 (1991).